

Water Resources Research®

RESEARCH ARTICLE

10.1029/2023WR035851

Key Points:

- We identify periods when streamflow anomalously often falls below/exceeds 5-year return period thresholds for 319 basins in Brazil
- Drought-rich periods were detected in 81% of the basins, while flood-rich periods were detected in 17% of the basins in 1940–2020
- The high drought frequency is caused by increased water abstractions and long-term rainfall deficits associated with climate modes

Supporting Information:

Supporting Information may be found in the online version of this article.

Correspondence to:

V. B. P. Chagas,
vbchagas@gmail.com

Citation:

Chagas, V. B. P., Chaffe, P. L. B., & Blöschl, G. (2024). Drought-rich periods are more likely than flood-rich periods in Brazil. *Water Resources Research*, 60, e2023WR035851. <https://doi.org/10.1029/2023WR035851>

Received 20 JUL 2023

Accepted 29 SEP 2024

Drought-Rich Periods Are More Likely Than Flood-Rich Periods in Brazil



Vinícius B. P. Chagas^{1,2} , Pedro L. B. Chaffe¹ , and Günter Blöschl²

¹Department of Sanitary and Environmental Engineering, Federal University of Santa Catarina, Florianopolis, Brazil,

²Institute of Hydraulic Engineering and Water Resources Management, Technische Universität Wien, Vienna, Austria

Abstract Streamflow exhibits persistent decadal variability; however, it is unclear if the magnitude and spatial extent of these variabilities are symmetric for droughts and floods. Here, we examine drought-rich and flood-rich periods in 319 streamflow gauges in Brazil from 1940 to 2020. Drought- and flood-rich periods are detected by computing annual streamflow minima and maxima time series and using scan statistics to verify if events exceeding a threshold follow a Bernoulli process. We contrast streamflow time clustering with rainfall, evaporation, water abstraction, the Atlantic Multidecadal Oscillation (AMO), and the Pacific Decadal Oscillation (PDO). We detected a higher spatial frequency of drought- than flood-rich periods. For 5-year return period thresholds, drought-rich periods are observed in 81% of the basins, 16.7 times the false positive rate (4.8%) and 4.7 times flood-rich periods (17%). This asymmetry is linked with sharp increases in water abstractions since the 1990s and a higher prevalence of rainfall-poor periods (41% of gauges) compared to rainfall-rich (22% of gauges), which we interpret as being further amplified into drought-rich periods due to an interannual persistence of water storage deficits. Brazil experienced a dry period until the 1960s, extensive flooding in the 1980s, and record low flows from the 2000s onward. Drought and flood-rich periods are well aligned with rainfall clustering, water abstractions, the AMO and PDO. Droughts-rich periods are more frequent in shorter time scales (several years to one decade) and flood-rich periods in longer time scales (a few decades). Our findings highlight the nonlinearity and asymmetry of drought and flood change at decadal scales.

1. Introduction

The magnitudes of droughts and floods have considerably changed worldwide in recent decades (Gudmundsson et al., 2021; Milly et al., 2015; Slater et al., 2021). These changes are often analyzed through linear trends spanning up to five decades, but as the analysis period increases, hydrometeorological time series start exhibiting decadal to multidecadal variabilities including abrupt shifts and temporal clustering (Blöschl et al., 2020; Cook et al., 2022; Kundzewicz et al., 2019; Markonis & Koutsoyiannis, 2016). Droughts and floods may be clustered into drought-rich and flood-rich periods, when they occur within a few decades rather than sparsely distributed over the century. Understanding how drought- and flood-rich periods arise and their causes remain an unsolved problem in hydrology (Blöschl, Bierkens, et al., 2019), suggesting that we should go beyond linear trend analyses as they may underestimate other forms of nonstationarity (Hannaford et al., 2013).

The temporal persistence of hydrometeorological time series has been observed across a range of time scales, from decades to millennia. Evidence indicates that, in the 20th century, meteorological drought-rich periods followed cycles of 12–13 years in Europe (Ionita et al., 2012), multidecadal variability in Australia (Kiem & Franks, 2004) and the US (McCabe et al., 2008; Seager, 2015), and cycles of 48 years in Thailand (Buckley et al., 2007). Similarly, flood-rich periods have been identified in Africa (Bola et al., 2022), Australia (Liu & Zhang, 2017), and Europe (Blöschl et al., 2020; Lun et al., 2020; Tarasova et al., 2023). However, the long-term persistence of precipitation time series is significantly larger in the southern hemisphere than in the northern hemisphere (O'Connell et al., 2022), leading to unusually long periods of above or below-average precipitation. In South America, hydrometeorological anomalies have been detected at multidecadal scales (García & Mechoso, 2005; Marengo et al., 2018; Saurral et al., 2017) and centennial scales in reconstructed paleoclimatic records (Bernal et al., 2016; Flantua et al., 2016; Morales et al., 2020; Vuille et al., 2012). Most South American anomalies have been linked with sea surface temperature variabilities in the Pacific and Atlantic oceans (Cavalcanti, 2012; Flantua et al., 2016; Grimm, 2019; Lima & AghaKouchak, 2017; Marengo et al., 2018), especially long-term variabilities in the Atlantic Multidecadal Oscillation (AMO) and Pacific Decadal Oscillation (PDO) (Grimm, 2019).

© 2024. The Author(s).

This is an open access article under the terms of the Creative Commons Attribution License, which permits use, distribution and reproduction in any medium, provided the original work is properly cited.

It is unclear, however, how drought-rich and flood-rich periods are linked with one another and if their occurrence is symmetric in terms of frequency, duration and spatial extent. While research has simultaneously investigated linear trends in droughts and floods (e.g., Chagas et al., 2022a; Ekolu et al., 2022; Gudmundsson et al., 2021), the concurrent analysis of streamflow drought-rich and flood-rich periods and their causes has not been conducted on a large-scale in Brazil, particularly over periods nearing a century. In this study, we address the following questions:

- (i) How frequent were drought-rich and flood-rich periods in Brazil from 1940 to 2020?
- (ii) What are their spatiotemporal characteristics?
- (iii) How are drought-rich and flood-rich periods linked with rainfall-rich periods, rainfall-poor periods, the AMO and the PDO?

We analyze observed daily streamflow data of 319 river basins and rainfall data of 312 gauges from 1940 to 2020. For each gauge, we compute the time series of minimum and maximum annual streamflow and detect drought-rich and flood-rich periods using scan statistics assuming a Bernoulli process (Lun et al., 2020). We analyze extreme events that exceed thresholds of 5, 10, and 20-year return periods. The causes of drought-rich and flood-rich periods are investigated using quasi-binomial regressions as a function of rainfall-rich periods, rainfall-poor periods, water use for irrigation and other purposes, and anomalies in the AMO and PDO.

2. Data and Methods

2.1. Data

We examine daily streamflow data from 319 river gauges (Figure 1c), selected out of the 3,679 river gauges available in the CAMELS-BR data set (Chagas et al., 2020a, 2020b). The gauges selected resulted from a data availability criterion of at least 60 years of data from 1940 to 2020, while ensuring that each year has at least 80% of the daily data available. This led to an analysis confined to the east of Brazil, as regions to the west such as Amazonia do not have long enough time series. We visually inspected the time series of each gauge, excluding from the analysis gauges with zeroes instead of missing data, orders of magnitude greater than expected, or abrupt changes tied to instrument changes or anthropogenic influence. Abrupt changes in streamflow from anthropogenic causes (changing measurement instruments) are identified by checking for abrupt changes in the stage-discharge relationship, conducted by visually inspecting the streamflow and river stage time series concurrently.

We analyze daily rainfall data from 312 rainfall gauges (Figure 1f), selected out of the 12,306 rainfall gauges available in the CAMELS-BR data set (Chagas et al., 2020a, 2020b) using the same data availability criterion as that for river gauges. While the CAMELS-BR data set also includes catchment-averaged rainfall time series from gridded precipitation data sets, here we restrict our analysis to data from rainfall gauges as they have longer time series and are more observation-based than gridded data sets. Furthermore, we restrict our investigation to rainfall gauges located within 50 km of the analyzed river basin boundaries. This constraint ensures a closer match between the spatial distribution of rainfall and river gauges and, on a large-scale analysis, a correspondence between rainfall gauges and individual catchments.

Daily evaporation (including transpiration) is incorporated into the rainfall time series by merging the rainfall gauge data with the evaporation gridded data from ERA5 (Hersbach et al., 2020). The ERA5 data set includes daily evaporation from 1940 to 2020 with a spatial resolution of 0.25° . For each rainfall gauge, we compute the rainfall minus evaporation time series by searching for the closest ERA5 cell and incorporating its evaporation data into the rainfall data.

The streamflow data are also contrasted with water use and sea surface temperature data. The consumptive water use data include water use for irrigation and other purposes that do not return to the basin (such as via evaporation or incorporation into products), spanning from 1940 to 2017 on an annual scale (ANA, 2019a). The sea surface temperature anomaly data from the AMO and PDO cover from 1940 to 2020 at a monthly time scale (Huang et al., 2017).

2.2. Study Area

The study area is confined to the southern and eastern parts of Brazil (about $2,000,000 \text{ km}^2$), which presents a climate gradient with higher mean annual rainfall minus evaporation in the south and lower values in the northeast

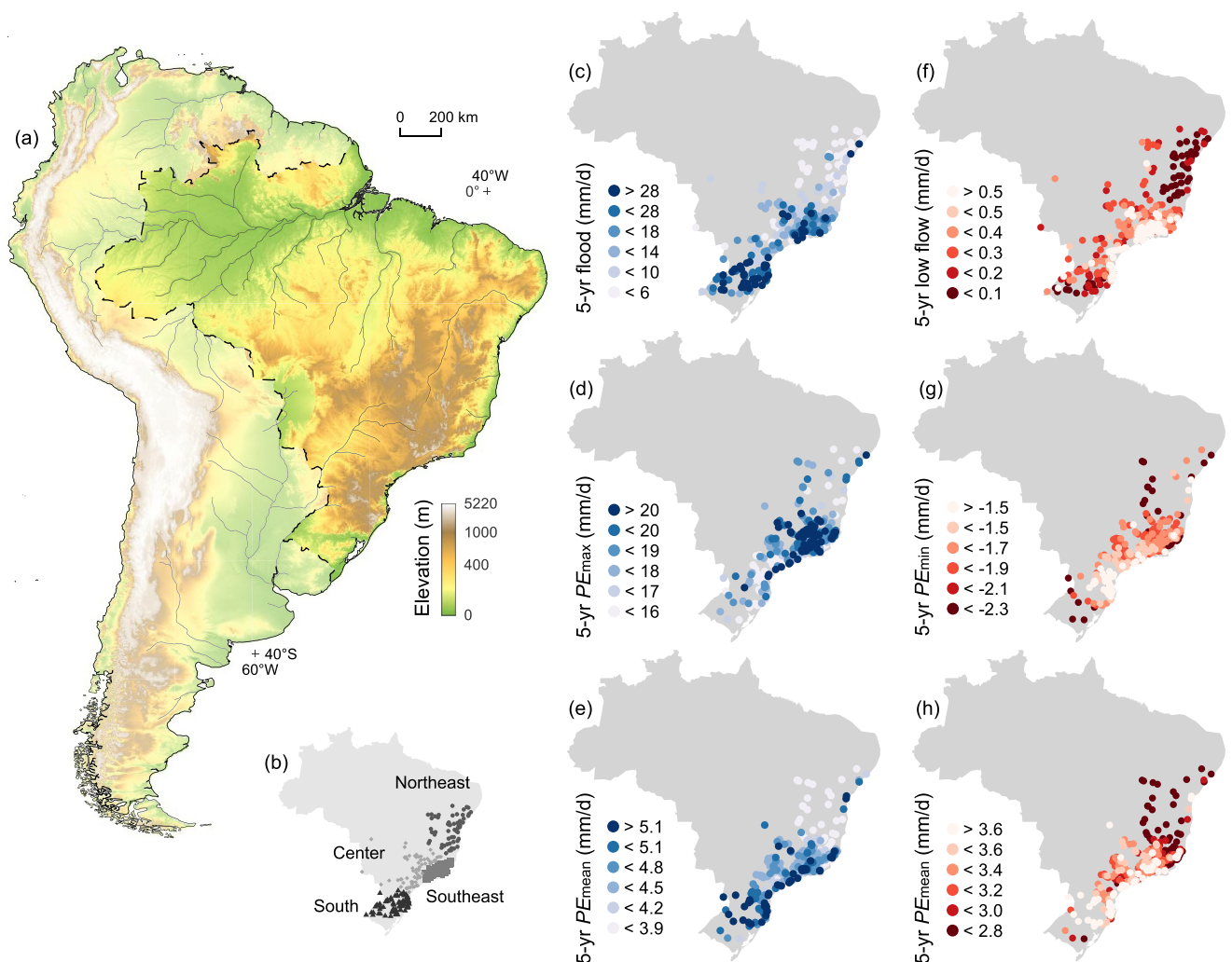


Figure 1. Study area and 5-year return period thresholds. (a) Brazilian topography. (b) Division of river gauges into regions. (c) Exceedance thresholds of 5-year return period (1940–2020) of floods (maximum annual streamflow), (d) PE_{\max} (maximum annual 14-day rainfall minus evaporation), and (e) PE_{mean} (mean annual rainfall minus evaporation). (f) Corresponding thresholds for when values drop below the 5-year low flows (minimum annual 7-day streamflow), (g) PE_{\min} (minimum annual 90-day rainfall minus evaporation), and (h) PE_{mean} .

(Figures 1e and 1h). The south has a temperate climate with low seasonalities, while the northeast includes portions with semiarid climates and high seasonalities. Between these regions, the climate is predominantly monsoonal with wet summers and dry winters. This monsoonal area can be divided into the southeastern region (Figure 1b), a mountainous region with higher humidity coming from the coast; and the central region, comprised of mostly highlands and continental climates. The catchments analyzed are mostly upstream of some of the largest Brazilian rivers (Figure 1a), which include the Uruguay, Iguaçu, Paraná, and São Francisco rivers. The catchment sizes range from 70 to 760,000 km², with a median of 1,860 km².

2.3. Detection of Flood-Rich and Drought-Rich Periods

We detect flood-rich and drought-rich periods using the scan statistics method of Lun et al. (2020). For each river gauge, we compute the time series of maximum annual daily flow magnitudes (water year starting in September) and minimum annual 7-day flow magnitudes (water year starting in March). A flood event is defined by when the maximum annual flow of a river basin exceeds a threshold defined by a recurrence interval, here computed for three scenarios of 5, 10, and 20-year return periods (Figure 1c shows 5-year thresholds for each gauge). Similarly, streamflow drought events are defined by when the minimum annual 7-day flow falls below its corresponding

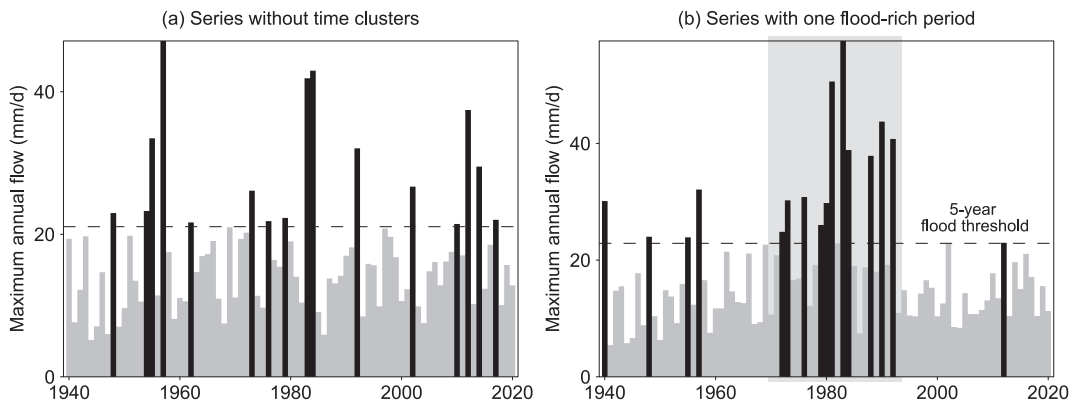


Figure 2. Example of a flood time series (a) without significant time clusters (gauge ID 83690000) and (b) with a significant flood-rich period ($p < 0.001$) (gauge ID 83440000). The dashed line is the 5-year return period threshold, black bars are flows above the threshold and gray bars are flows below the threshold. The shaded area in (b) shows the window when the flood-rich period was detected.

return period thresholds (Figure 1f). The thresholds are estimated with order statistics (Makkonen & Pajari, 2014) as it does not assume a distribution, is less prone to bias, and allows for an exact count of flood and drought events at each time series depending on its length and the return period. Given a median length of the annual time series of 80 years, the three return period scenarios lead to a total of 16, 8, and 4 flood and drought events for each gauge analyzed. Furthermore, the annual time series in certain gauges contain years without data, which we interpolated using linear regression with the highest correlated gauge as a donor. Each river gauge had an average of 5.9 years of data filled, or 7.3% of the time series. The rainfall indices (better described in Section 2.5) had on average 6.1 years filled, or 7.5% of the time series.

Flood-rich and drought-rich periods are defined by when the occurrence of floods and droughts within a time window deviates from a reference condition of independently and identically distributed series, as modeled by a Bernoulli process (Lun et al., 2020). In other words, these are periods when flood and drought occurrences are significantly clustered in time. Within a time window of w years, the number of successes in Bernoulli trials (here annual floods or droughts above or below a threshold) follows a binomial distribution, which is used to compute its probability distributions. To fully assess whether a significant flood or drought-rich period exists in a time series, binomial probabilities must consider multiple window sizes and running windows from the beginning to the end of series. A complete description of this procedure is available in Lun et al. (2020). Some examples of computed probabilities are available in Table A1 for 5-year return period thresholds.

Given an annual time series of length n , we compute the number of flood events (or droughts) observed in each window of w years that runs from the start to the end of the series. We scan for and identify the window with the highest event count, marking it as a potential flood-rich or drought-rich period. The probability of occurrence of k or more events within a window, given that a events are observed over the entire time series, is denoted by $P(k|w, n, a)$. A larger number of k events within a window correlates with lower probabilities and, if below a significance level α , indicates a significantly anomalous flood-rich or drought-rich period. Thus, flood occurrence (or drought) in a river basin can be either sparsely distributed over the years without a significant time cluster, such as the example shown in Figure 2a, or include a significant flood-rich period (or drought) such as in Figure 2b, where 11 out of 16 floods (1940–2020) were clustered within a 24-year window from 1970 to 1993.

We consider different window sizes for the return periods of 5 years ($w = 6, 9, 12, 16, 20, 24, 28$, and 33 years), 10 years ($w = 7, 13, 21$, and 31 years), and 20 years ($w = 7$ and 21 years). This is because the results vary considerably depending on the significance level (α) chosen (not shown). The number of significant flood-rich (or drought) periods relative to α is inflated for lower α , particularly those below 0.01. Thus, for comparable results between window sizes and return periods, we selected only window sizes with probabilities close to 0.05, even though they are never exactly 0.05 due to the discrete nature of the method. Given that the window size of flood and drought-rich periods is not known a priori, Lun et al. (2020) consider multiple windows concurrently by computing the complementary probabilities of not having significant results in all windows. Thus, the frequencies

of significant flood and drought-rich periods presented here consider all windows concurrently, unless noted otherwise.

2.4. Controlling for the False Discovery Rate

Once the number of gauges with significant flood and drought-rich periods is identified, we apply the false discovery rate (FDR) controlling procedure to address the overestimation of significant results when repeating an individual statistical test on multiple sites (Wilks, 2006), for an evaluation of field significance (Renard et al., 2008), and for a robust analysis to data with high spatial dependency (Wilks, 2016). The FDR is defined as the expected proportion of incorrectly rejected local null hypotheses among all rejections (Benjamini & Hochberg, 1995), which is used to address the increased likelihood of false discoveries when the test is repeated across multiple sites (Wilks, 2006). We control for the FDR with the Benjamini and Hochberg (1995) procedure, which compensates for such hypothesis testing biases including in data sets with high spatial dependence (Renard et al., 2008; Wilks, 2016). The field significance can be assessed by checking if at least one gauge in a particular study area or region displays a significant rejection of the null hypothesis (Renard et al., 2008; Wilks, 2016). Furthermore, the FDR controlling procedure tends to result in an underestimation of significant null hypothesis rejections for scenarios of high dependence (Wilks, 2016), which we compensate for by adopting an FDR significance level (α_{FDR}) of two times the local significance level (α), as proposed by Wilks (2016).

2.5. Investigating the Causes of Flood-Rich and Drought-Rich Periods

We explore relationships between flood-rich and drought-rich periods with rainfall, evaporation, water use, and sea surface temperature by contrasting their spatiotemporal patterns, grouping the gauges into regions, and applying quasi-binomial regression models for the count of gauges with time clusters in each region.

In the first step, we investigate rainfall-rich and rainfall-poor periods at each rainfall gauge (including evaporation) with various indices: PE_{\max} -rich periods using maximum annual 14-day rainfall (P) minus evaporation (E) time series (Figure 1d); PE_{mean} -rich (abnormally wet mean annual $P - E$, Figure 1e); PE_{\min} -poor (abnormally dry minimum annual 90-day $P - E$, Figure 1g); and PE_{mean} -poor (abnormally dry mean annual $P - E$, Figure 1h). The PE_{\max} -rich, PE_{mean} -rich and PE_{mean} -poor time series are computed with the water year starting in September; and the PE_{\min} -poor series are computed starting in March. Similar indices have been linked with drought and flood changes in Brazil in the past four decades (Chagas et al., 2022a) and in other studies (e.g., Blöschl, Hall, et al., 2019), allowing easier comparison of the results. We chose the time scale of 14 days for PE_{\max} as a compromise between time scales relevant to floods in small and large catchments. We highlight that the results are robust to this choice, considering that the time series of 14-day PE_{\max} are highly correlated with 7-day PE_{\max} (median Spearman correlation of 0.84) and 30-day PE_{\max} (median Spearman correlation of 0.85). On the other hand, the time scale of 90 days for PE_{\min} aims to investigate droughts linked with seasonally dry periods, in contrast to the annual scale of PE_{mean} which focuses on longer dry periods linked with the annual meteorological water balance.

We group rainfall and river gauges into four regions with similar climates: South (temperate climate with low seasonality); Center (tropical monsoonal climate); Southeast (tropical coastal and mountainous climates); and Northeast (semiarid). This division is based on expert reasoning rather than a formal statistical procedure. Grouping into large-scale regions lets us focus on the climatic component of floods and droughts and limit local-scale impacts of artificial regulation and anthropogenically induced changes. In each region, we count the number of gauges with significant flood-rich, drought-rich, rainfall-rich and rainfall-poor periods at each year.

Finally, we use quasi-binomial regressions for each region to estimate flood-rich counts as a function of PE_{\max} -rich and PE_{mean} -rich counts. Drought-rich counts are estimated as a function of PE_{\min} -poor, PE_{mean} -poor, and the average water use relative to the mean annual streamflow. Similar quasi-binomial regression models are used to explore links between flood- and drought-rich counts, the AMO and the PDO, the last two analyzed as long-term anomalies from a 241-month moving average. The 241-month time scale is chosen because of the highest explanatory power compared to other time scales (Figure S1), even though the regression coefficients are robust across time scales (not shown).

The quasi-binomial regressions between streamflow and rainfall are computed with a linear link between the dependent and independent variables, as count data are present on both sides of the equation and the water use

Table 1

Frequency of Gauges With Significant Drought-Rich Periods (Minimum Annual 7-Day Flow), Flood-Rich (Maximum Annual Daily Flow), PE_{max} -Rich (Maximum Annual 14-Day Rainfall (P) Minus Evaporation (E)), PE_{mean} -Rich (Mean Annual $P - E$), PE_{min} -Poor (Minimum Annual 90-Day $P - E$), and PE_{mean} -Poor Periods From 1940 to 2020

| Variable | Total no. of gauges | Frequency of sig. gauges (%) | Expected (%) | Frequency/expected (-) |
|-------------------|---------------------|------------------------------|--------------|------------------------|
| Drought-rich | 319 | 80.9 | 4.83 | 16.7 |
| PE_{min} -poor | 312 | 25.6 | 4.85 | 5.3 |
| PE_{mean} -poor | 312 | 23.7 | 4.88 | 4.9 |
| Flood-rich | 319 | 17.2 | 4.91 | 3.5 |
| PE_{max} -rich | 312 | 7.7 | 4.89 | 1.6 |
| PE_{mean} -rich | 312 | 17.0 | 4.92 | 3.5 |

Note. Frequencies consider all window sizes and are controlled for the false discovery rate. The expected values represent the local significance level (type I error) and the last column is the ratio of the observed frequency to what would be expected by chance. The values presented are for 5-year return period thresholds.

data follows an exponential distribution. In contrast, the regressions between streamflow and sea surface temperature are analyzed with a logit link. The quasi-binomial model is appropriate for our data as it has distinct parameters for the mean and variance, in contrast with the binomial model. Standard errors are calculated using robust covariance matrix estimators (MacKinnon & White, 1985). The statistical significance of coefficients is analyzed with z -scores, computed as the ratio of the coefficient estimate to the standard error. The regressions' goodness of fit is evaluated using a pseudo R^2 of McFadden (1973), which cannot be interpreted as the variance explained by the model. We examined alternative regressions that include interactions among the terms, with results close to those presented here (not shown). In the regression using sea surface temperature, we detrend the drought-rich and flood-rich frequencies to match the detrended AMO and PDO time series (Huang et al., 2017). The detrending was conducted with ordinary least squares regression. For an easier interpretation of the regression coefficients, we transform the AMO and PDO time series into z -scores by dividing by their standard deviations and centralizing with their means.

3. Results

3.1. Frequency of Drought-Rich and Flood-Rich Periods

Basins with significant streamflow drought-rich periods were 4.7 times more frequent as those with flood-rich periods between 1940 and 2020 (Table 1; average significance level α of 0.049 for floods and droughts). This ratio considers droughts and floods that exceed a 5-year return period threshold and a statistical significance considering all window sizes, ensuring that the same total number of droughts and floods are identified in each time series. Drought-rich periods were observed in 80.9% of the basins, 16.7 times higher than the expected value from the type I error of 4.83% while controlling for the false detection rate. In contrast, flood-rich periods occurred in 17.2% of the basins, 3.5 times the expected value. This flood-rich frequency is similar to those found in Europe, which range from 2 to 4 times above the expected value (Lun et al., 2020; Merz et al., 2016). Overall, 84.0% of the basins had either a significant drought- or flood-rich period, with 14.1% experiencing both drought- and flood-rich periods although mostly non-concurrent. Thus, for the past 80 years, the assumption of independently and identically distributed series, commonly used in statistical hydrology, is not met in most river basins.

Rainfall-rich and -poor periods (including evaporation) were also widely detected (Table 1). A total of 40.7% of the rainfall gauges recorded a significant rainfall-poor period (i.e., either a significant PE_{min} -poor or PE_{mean} -poor period). Both rainfall indices are associated with streamflow droughts as, in the tropics, they are commonly caused by the dry season immediately before the drought (PE_{min} -poor) or by abnormally low rainfall year-round and in the previous wet season resulting in reduced groundwater recharge volumes (PE_{mean} -poor) (Van Loon & Van Lanen, 2012). In contrast, 21.5% of the gauges recorded a significant rainfall-rich periods (i.e., either a significant PE_{max} -rich or PE_{mean} -rich period), which could lead to floods through extreme rainfall events (PE_{max} -rich) or abnormally wet years resulting in humid soils (PE_{mean} -rich) (Chagas et al., 2022b).

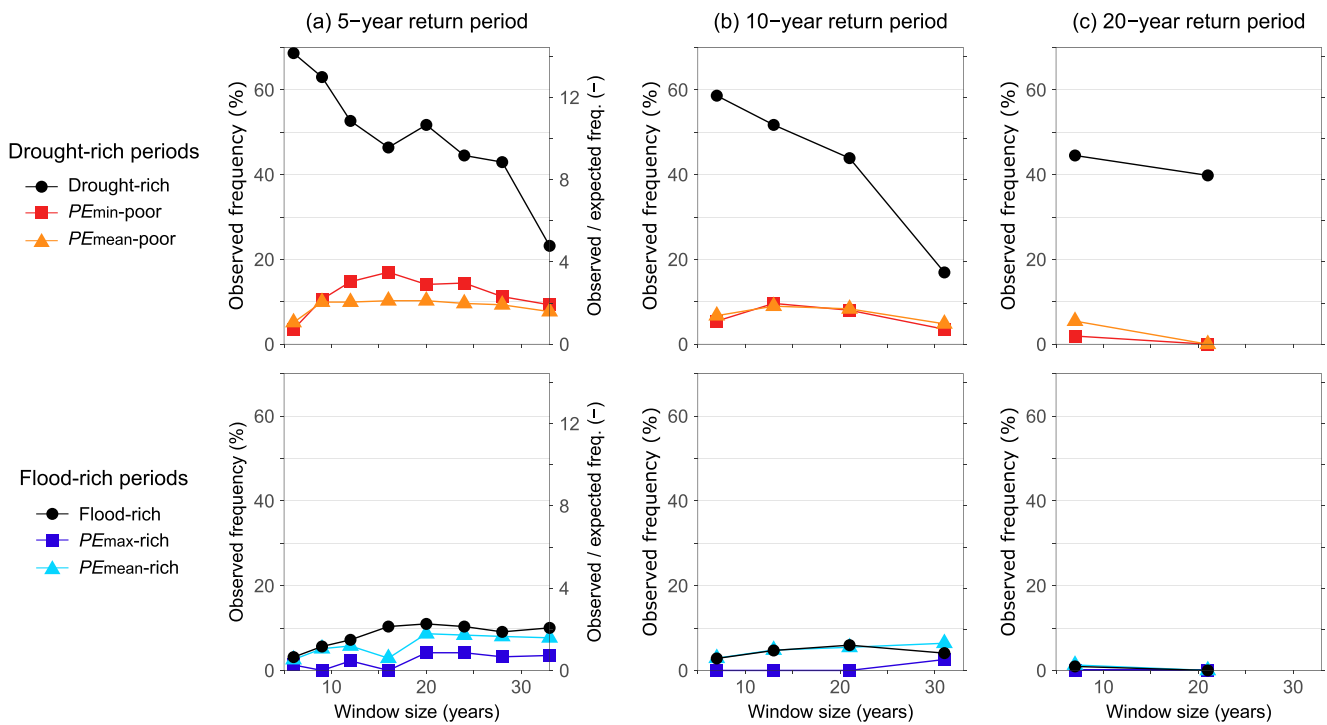


Figure 3. Frequency of gauges with significant drought-rich, flood-rich, rainfall-rich, and rainfall-poor periods as a function of the running window size (i.e., the time scale) and return period thresholds of 5, 10, and 20 years.

The number of gauges with time clusters is notably related to the return period threshold (Figure 3). The frequency of time clusters decreases for higher return periods (Figure 3), that is, as the thresholds for droughts and floods get more restrictive. Drought-rich periods were detected in at least one window size in 80.9% of the basins considering 5-year droughts, 69.0% for 10-year droughts, and 54.2% for 20-year droughts. For floods, these values are 17.2%, 7.8%, and 0.9%. Such a low number of gauges with flood-rich frequencies at higher thresholds (20-year return periods), in agreement with Lun et al. (2020) and Merz et al. (2016), might indicate either that the most extreme floods truly do not cluster in time often or that longer time series are necessary for a more accurate evaluation. Longer time series may reveal further flood-rich periods, given that considerable clustering has been observed in Europe when investigating data spanning a few centuries (Blöschl et al., 2020). A similar pattern is observed for rainfall extremes.

Drought and flood-rich periods have the opposite relationship with the time scale investigated (i.e., the window size) (Figure 3). Drought-rich periods are more common at shorter time scales, while flood-rich periods are more common at longer time scales. For a 5-year return period threshold, drought-rich periods are most frequent at a window size of 6 years (68.7% of the gauges) and least frequent in a window of 33 years (23.2%) (Figure 3a). On the other hand, flood-rich periods are less frequent at a window of 6 years (3.1%), peaking at a window size of 16 years and becoming stable at longer window sizes (Figure 3a). This relationship is not observed for the rainfall indices, which have low clustering frequencies at the smallest window size but stable frequencies afterward. These results suggest that extreme droughts often occur in a sequence of a few years, while extreme floods often occur in a sequence of a few decades.

3.2. Spatiotemporal Distribution of Drought-Rich and Flood-Rich Periods

Both drought and flood-rich periods were detected across most of the study area (Figures 4a, 4d, and 4g), showing that none of the regions explored is free from temporal clustering in the streamflow extremes. The same is observed for rainfall time clustering, although mostly for time scales longer than 6 years (Figure 4). Most variations in the streamflow and rainfall clustering are observed in time rather than in space.

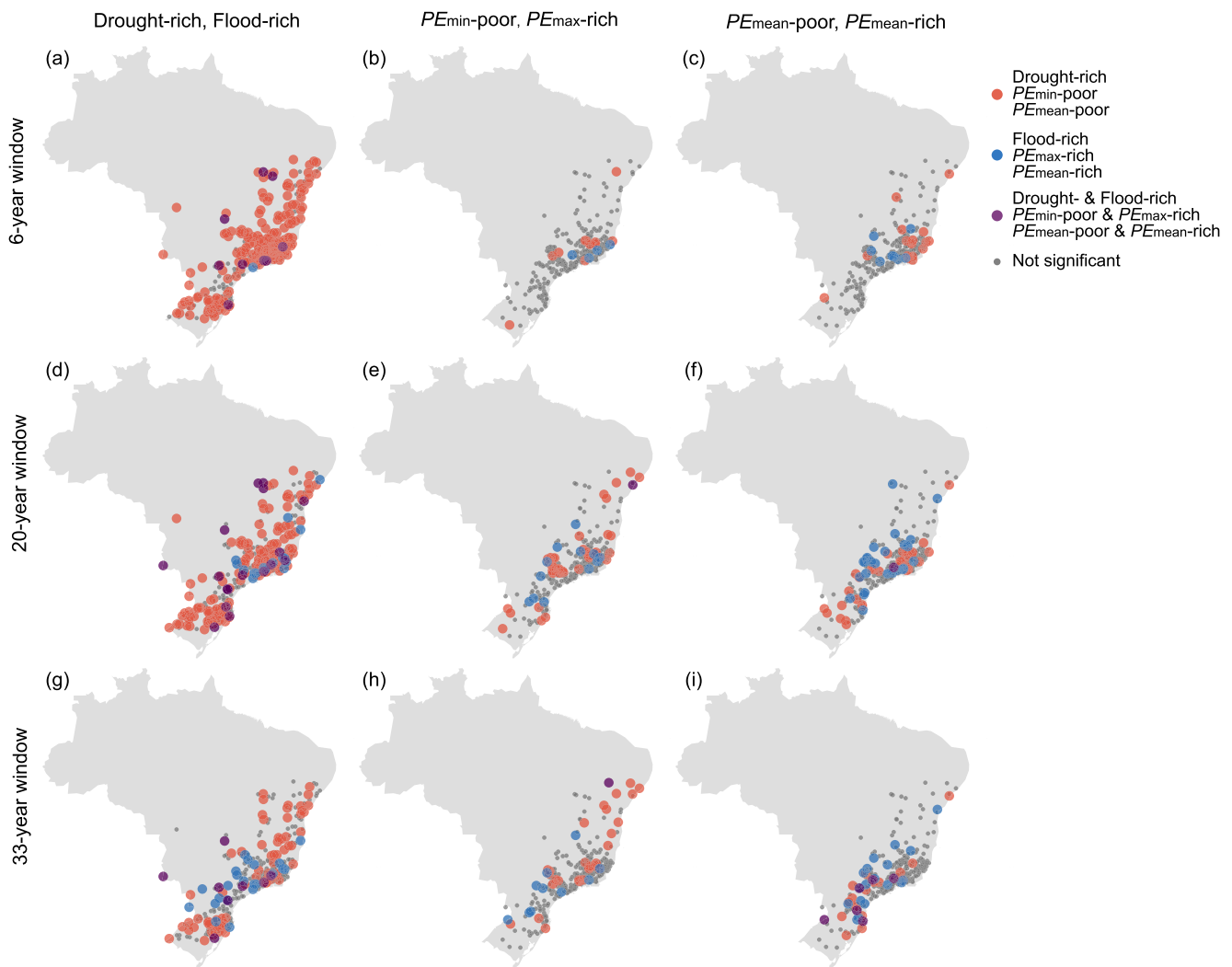


Figure 4. Spatial distribution of gauges with significant time clusters for (a–c) 6-year windows, (d–f) 20-year windows, and (g–i) 33-year windows, considering 5-year return period thresholds and a time cluster at any time from 1940 to 2020.

Drought-rich and flood-rich periods have changed considerably over time since 1940, exhibiting three main cycles: a dry period in the initial decades; a shift in the late 1970s with frequent flooding; and another reversal in the 2000s marked by a predominance of droughts. The temporal evolution can be seen in Figure 5, showing the spatial distribution of time clusters in each decade, and in Figure 6 which displays the number of gauges with a significant time cluster in each year in four regions.

The first dry period extends from the 1940s to the 1960s (Figure 5), with a peak number of gauges with significant drought-rich periods in the 1950s (Figure 6). The drought-rich periods are typically aligned with rainfall-poor periods, more prevalent in the south (Figure 6c) and less frequent in the southeast (Figure 6a). However, most records of this period's socioeconomic impacts refer to the northeast, as it is the most arid and susceptible region, with consequences such as mass emigration and economic losses (Marengo et al., 2017; Ponce, 1995).

The dry period was reversed in the late 1970s and early 1980s, with an increased number of gauges with flood-rich periods mainly in the central and northeastern regions (Figures 6d and 6b). The 1980s was the wettest period in a large part of Brazil since 1940, witnessing some of the largest floods recorded (Fleischmann et al., 2020). The shift from dry to wet period started with an increase in rainfall-rich periods, linked with a shift in the PDO in the late 1970s (Carvalho et al., 2011; Jacques-Coper & Garreaud, 2015), later followed by flood-rich periods. This

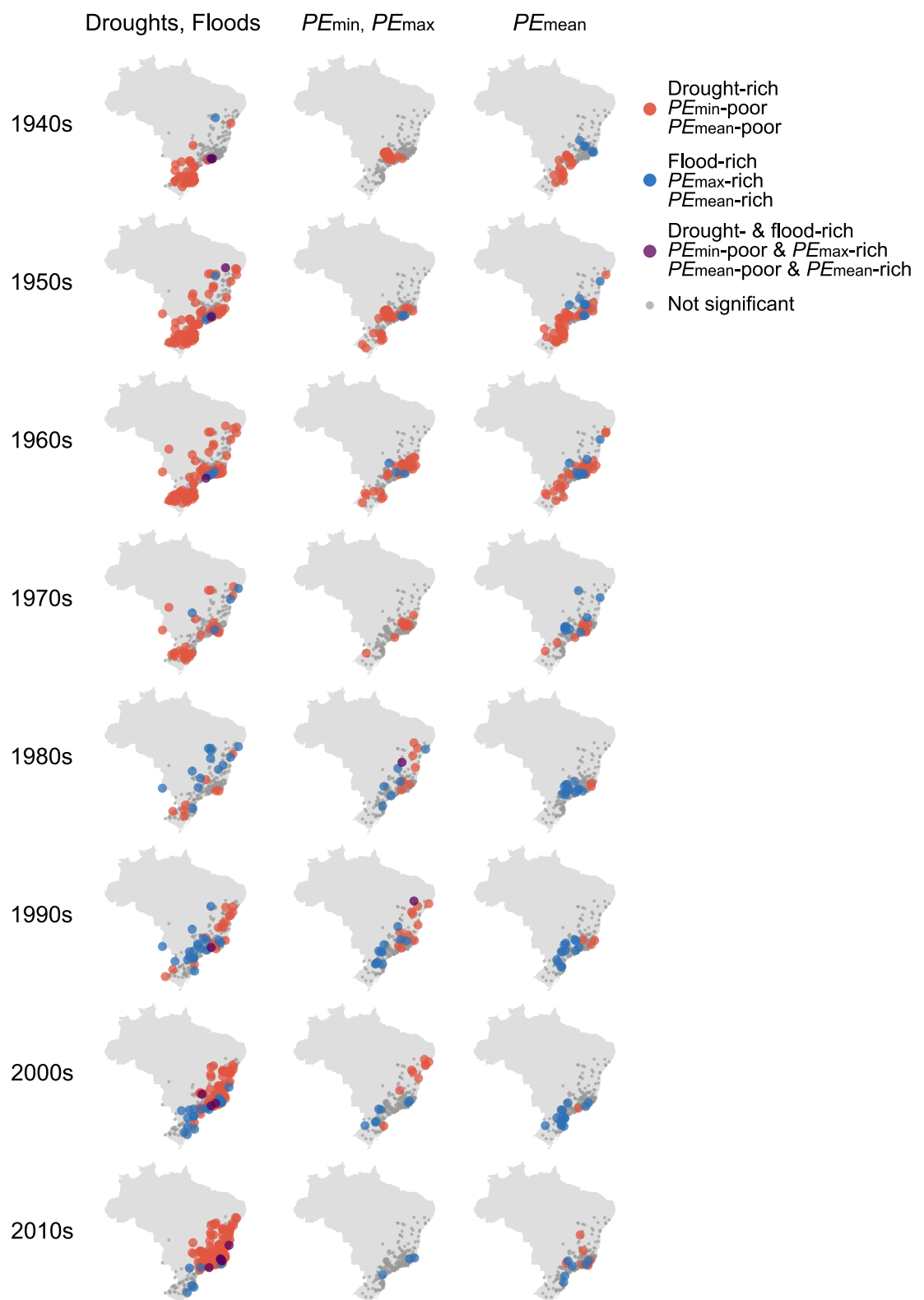


Figure 5. Spatial distribution of gauges with a significant time cluster in each decade, with 5-year return period thresholds and a significance considering all window sizes. The gauges with significant clusters are plotted only in the decade that includes the central year of the clustering window.

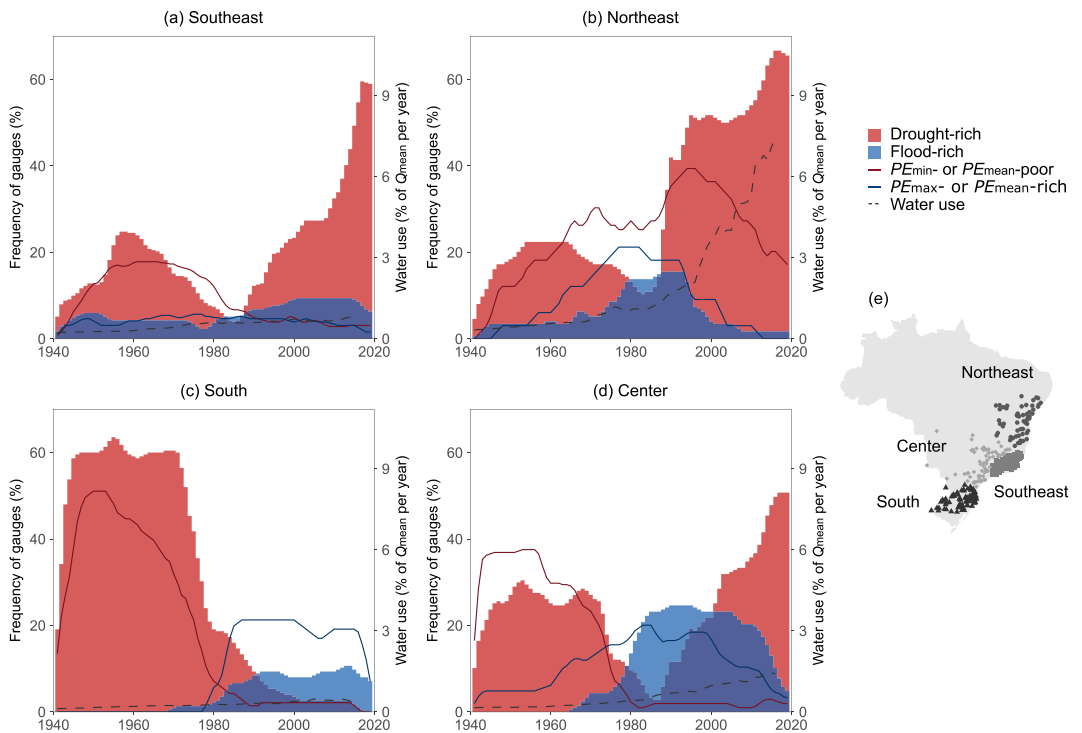


Figure 6. Time series of the frequency of gauges with significant drought-rich, flood-rich, rainfall-rich and rainfall-poor periods in (a) the southeast (number of river gauges $n_q = 117$, number of rainfall gauges $n_p = 129$), (b) northeast ($n_q = 58$, $n_p = 33$), (c) south ($n_q = 75$, $n_p = 47$), and center ($n_q = 69$, $n_p = 103$). Each year counts the number of gauges that were in a significant time cluster with 5-year return period thresholds and considering all window sizes.

delay between the rainfall-rich and flood-rich periods suggests that catchments may take several years to recharge the groundwater deficit accumulated from previous droughts.

The second dry period started in the 2000s, with an increased frequency of gauges with drought-rich periods in every region except for the south (Figure 6). More basins with significant drought-rich periods were recorded in the second dry cycle than in the first dry cycle, with frequencies of up to 67% of the gauges in the northeast region, 60% in the southeast, and 51% in the center (Figure 6). Streamflow in the 2010s often reached record lows (Cuartas et al., 2022; Getirana et al., 2021), resulting in severe water crises like those in São Paulo in 2014–2015 (Braga & Kelman, 2016) and partial disruption of the national hydropower generation (Tomasella et al., 2022). However, rainfall-poor periods were not as frequent as drought-rich periods after 2000. The higher frequency of drought-rich basins can be related to a combination of lower rainfall volumes (which are insufficient for a significant rainfall-poor period) and a rapid increase in water abstractions. This is especially evident in the central (Figure 6d) and northeastern regions (Figure 6b), which aligns with the linear trend analysis of Chagas et al. (2022a) for the period 1980–2015. Furthermore, a part of Brazil, close to the Doce river basin in the southeast, experienced an increase in both drought-rich and flood-rich periods simultaneously (Figure 5), suggesting that the acceleration of the water cycle (Chagas et al., 2022a) may be perceptible even in the most extreme flood and drought events.

3.3. Links With Rainfall, Water Use, and Sea Surface Temperature

The four regions analyzed had overall a good alignment between the time series of drought-rich periods, rainfall-poor periods and water use in terms of quasi-binomial regressions (Figure 7a). Results show a higher importance of PE_{mean} -poor over PE_{\min} -poor periods in all regions except for the south, suggesting that drought clusters are primarily linked with decreases in groundwater recharge in the wet season than with rainfall deficits in the dry season. This is in agreement with the controls of low flows in Brazil proposed by Chagas et al. (2024). In the

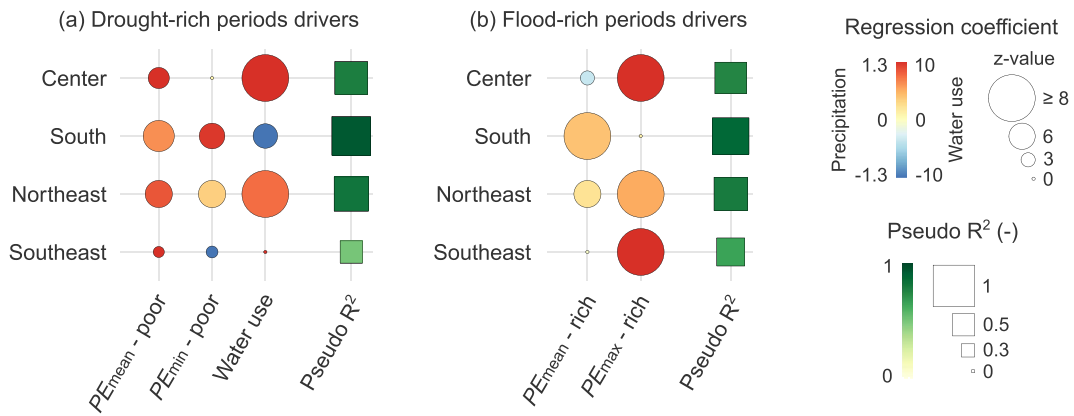


Figure 7. Quasi-binomial regression coefficients for (a) the frequency of gauges with drought-rich periods in each region as the dependent variable and $PE_{\text{mean-poor}}$, $PE_{\text{min-poor}}$, and consumptive water use as independent variables. (b) Coefficients for the regressions between flood-rich periods, $PE_{\text{mean-rich}}$ and $PE_{\text{max-rich}}$ periods. Flood and drought variables are computed based on a 5-year return period threshold. The regressions are computed with a linear link between the variables. Larger squares and darker green colors indicate higher pseudo R^2 .

northeast, the frequency of gauges with drought-rich periods is well predicted by the frequency of $PE_{\text{mean-poor}}$ periods and water use (pseudo R^2 of 0.81, $p < 0.01$), with a noticeable increase in water use from the late 1990s onward (Figure 6b). In the south, the frequency of drought-rich periods mirrors rainfall-poor periods (pseudo R^2 of 0.93, $p < 0.01$), with a negative impact of water use although not relevant because of its low coefficient and low water use over the years. The central region has a result similar to the northeast, while the southeast has the lowest regression coefficients and explanatory power (pseudo R^2 of 0.50, $p < 0.01$).

Flood-rich periods are well aligned with rainfall-rich periods in the four regions (Figure 7b). Water use is not included in the equation, as it is not significant for flood changes in Brazil (Chagas et al., 2022a). Flood-rich periods are linked mostly with $PE_{\text{max-rich}}$ periods in the center (pseudo R^2 of 0.74, $p < 0.01$), northeast (pseudo R^2 of 0.79, $p < 0.01$), southeast (pseudo R^2 of 0.65, $p < 0.01$). On the other hand, flood-rich periods are linked mostly with $PE_{\text{mean-rich}}$ in the south (pseudo R^2 of 0.87, $p < 0.01$).

Drought and flood-rich periods are significantly associated with 241-month anomalies in the AMO and PDO in the four regions analyzed. Drought-rich periods have pseudo R^2 ranging from 0.51 to 0.75; flood-rich periods have pseudo R^2 ranging from 0.54 to 0.77 (Figure 8). Increased drought-rich periods are related to cold PDO phases in the center, south, and southeast of Brazil regions (Figure 8c); and to warm AMO phases in the northeast. Conversely, increased flood-rich periods are linked with warm PDO phases in the center, south, and northeast; warm AMO phases in the south and southeast; and cold AMO phases in the northeast. The streamflow clustering is less explained by the AMO and PDO than by rainfall clustering, which shows influences of other climate modes such as the Southern Annular Mode (Morales et al., 2020), El Niño-Southern Oscillation (Kayano et al., 2013; Tedeschi et al., 2015), Madden-Julian Oscillation (Grimm, 2019), and others including hidden climatic indices (Renard & Thyer, 2019; Renard et al., 2022).

4. Discussion

The results suggest that the decadal clustering of streamflow extremes is considerably asymmetric for droughts and floods. Streamflow drought-rich periods are more spatially frequent than flood-rich periods, especially for smaller time scales such as 10 years or less. This finding holds even after ensuring the exact same number of droughts and floods in every time series and accounting for varying return period thresholds. From our perspective, the asymmetry is linked with three main factors: a higher frequency of time clustering of rainfall-poor periods than rainfall-rich periods; a stronger carry-over effect of streamflow droughts than floods with an interannual persistence of water storage deficits; and an amplification of streamflow droughts due to water abstractions.

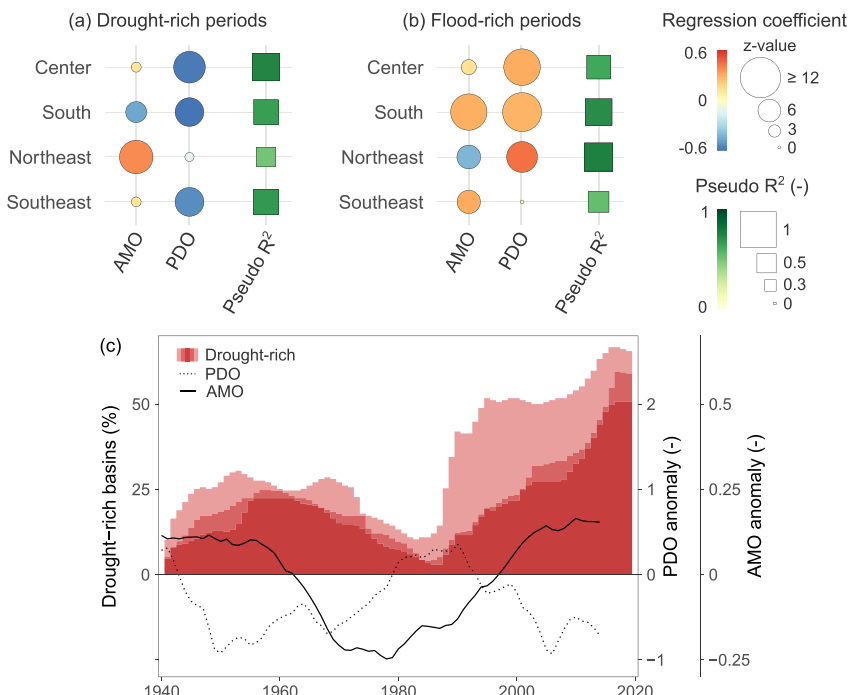


Figure 8. Quasi-binomial regression coefficients for (a) the frequency of gauges with drought-rich periods in each region as the dependent variable and 241-month anomalies in the Atlantic Multidecadal Oscillation (AMO) and Pacific Decadal Oscillation (PDO). (b) Coefficients for the regressions between flood-rich periods, AMO, and PDO anomalies. The regressions are computed with a logit link between variables. (c) Time series of AMO, PDO, and the frequency of drought-rich gauges in the southeast, northeast, and center regions. Flood and drought variables are computed based on a 5-year return period threshold.

Twice as many rainfall-poor periods were observed (40.7% of gauges, mostly in 1940–1970) compared to rainfall-rich periods (21.5% of gauges, mostly in 1980–2000). The causes of this discrepancy are not entirely understood and provide opportunity for further research. We find, however, that the climate index with the lowest number of temporal clustering is linked with extreme rainfall events (i.e., maximum annual 14-day rainfall minus evaporation). This is a considerable contributor to the lower frequency of flood-rich periods, particularly considering that flood-rich periods are linked mainly to clustering in extreme rainfall (Figure 7b).

Rainfall anomalies accumulate as basin water storage over months and years, resulting in a higher persistence of streamflow compared to rainfall time series (de Lavenne et al., 2022). This carry-over effect of water storage between years contributes to a higher frequency of basins with streamflow time clusters than rainfall time clusters, especially at short time scales. For instance, for 6-year windows and 5-year return period thresholds, drought-rich periods were observed at 68.7% of gauges even though rainfall-poor periods occurred in only 7.8% of the gauges. Generally, the persistence of low flows is even higher than high flows (e.g., David et al., 2022; McMillan, 2022), potentially contributing to a higher frequency of drought-rich than flood-rich periods, as a sequence of short-lived meteorological droughts gets pooled into longer hydrological droughts (Bevacqua et al., 2021; Mtilatila et al., 2020; Van Loon, 2015).

Water abstractions contribute to an increase in streamflow droughts in many regions of the world (Custodio, 2002; Di Baldassarre et al., 2018), amplifying the frequency of drought-rich periods even further. In Brazil, 68% of the total water use in 2017 was for irrigation purposes (ANA, 2019b). Irrigated agriculture expanded from 15 to 70 thousand km² from 1980 to 2015 (ANA, 2019a), with an increase in crop productivity leading to even more irrigation. Water abstractions are particularly high in the dry season, which generally lasts from 4 to 6 months (Grimm, 2019), contributing to the lowering of groundwater tables and dry-season flows (Chagas et al., 2022a). We note, however, that the impact of water use on drought-rich periods might be underestimated in our study because it does not consider evaporation from artificial reservoirs' lakes (ANA, 2019b). Water use is

potentially underestimated particularly in the driest areas of the northeast, where potential evaporation is higher and its numerous small reservoirs are often unmonitored (ANA, 2018).

The connection between streamflow time clustering and long-term sea surface temperature anomalies suggests that streamflow extremes might often undergo nonlinear changes. For example, the PDO consists of quasi-periodic cycles of 20 years (d'Orgeville & Peltier, 2007), marked by extended periods of opposite phases and rapid transitions between them (Newman et al., 2016), such as that of the late 1970s (Carvalho et al., 2011; Jacques-Coper & Garreaud, 2015). Thus, studies of drought and flood change would benefit from considering nonstationarities such as cycles and step changes. In this regard, the analysis of drought-rich and flood-rich periods (Blöschl, Bierkens, et al., 2019; Lun et al., 2020) shows promising results and an opportunity for exploring the causes of such decadal variabilities.

5. Summary and Conclusions

In this study, we investigate streamflow drought-rich and flood-rich periods (i.e., interannual time clustering of droughts and floods) in Brazil from 1940 to 2020. We looked at their association with rainfall-poor and rainfall-rich periods, water abstractions, the AMO and the PDO. Considering events that exceed 5-year return periods, we found that gauges with significant ($\alpha = 0.049$) drought-rich periods were 4.7 times as frequent in space as flood-rich periods, even after ensuring an equal number of droughts and floods for each time series. We detected drought-rich periods in 80.9% of the gauges analyzed, 16.7 times higher than expected by chance. It shows how the most severe droughts of the century often cluster into periods of one to two decades, indicating that the assumption of independently and identically distributed series does not hold in most river basins. We believe that the asymmetry between drought- and flood-rich periods is linked to increased water abstractions and a higher frequency of rainfall-poor periods than rainfall-rich periods, which we interpret as being further amplified into drought-rich periods through a persistence of water storage deficits between years.

The large-scale patterns of drought and flood-rich periods are well predicted either by rainfall clustering and water abstractions (pseudo R^2 ranging from 0.50 to 0.93) or by the AMO and PDO (pseudo R^2 from 0.51 to 0.77). In general, Brazil experienced a dry period from the 1940s to the 1960s, a wet period in the 1980s and 1990s with the largest floods on record (Fleischmann et al., 2020), and another dry period from the 2000s onward with record low flows. The current dry period has been linked with water abstractions (Chagas et al., 2022a) and to a partial disruption of the national hydropower generation (Tomasella et al., 2022). These multidecadal cycles are associated with 241-month anomalies in the AMO and PDO, characterized by extended periods of opposite phases with rapid transitions between them (Newman et al., 2016).

Our findings suggest that drought and flood change investigations can benefit from analyzing nonlinear changes, especially for periods nearing one century. The analysis of drought-rich and flood-rich periods (Blöschl, Bierkens, et al., 2019; Lun et al., 2020) shows promising results, particularly when considering asymmetries of decadal drought and flood variabilities.

Appendix A

See Table A1.

Table A1

Probabilities of Occurrence $P(k|w,n,a)$ of k or More Events Within a Window w , Sized From 5 to 16 Years, in a Time Series of Length $n = 80$ Years (the Median Length for River Gauges) and $a = 16$ Total Events Over the 80 Years (i.e., Events Above a 5-Year Return Period Threshold)

| k (events) | $w = 6$ | $w = 7$ | $w = 8$ | $w = 9$ | $w = 10$ | $w = 11$ | $w = 12$ | $w = 13$ | $w = 14$ | $w = 15$ | $w = 16$ |
|--------------|----------------------|----------------------|----------------------|----------------------|----------------------|----------------------|-----------------------|-----------------------|-----------------------|-----------------------|----------|
| 1 | 1.000 | 1.000 | 1.000 | 1.000 | 1.000 | 1.000 | 1.000 | 1.000 | 1.000 | 1.000 | 1.000 |
| 2 | 1.000 | 1.000 | 1.000 | 1.000 | 1.000 | 1.000 | 1.000 | 1.000 | 1.000 | 1.000 | 1.000 |
| 3 | 1.000 | 1.000 | 1.000 | 1.000 | 1.000 | 1.000 | 1.000 | 1.000 | 1.000 | 1.000 | 1.000 |
| 4 | 0.985 | 0.998 | 1.000 | 1.000 | 1.000 | 1.000 | 1.000 | 1.000 | 1.000 | 1.000 | 1.000 |
| 5 | 0.428 | 0.627 | 0.790 | 0.900 | 0.961 | 0.988 | 0.997 | 1.000 | 1.000 | 1.000 | 1.000 |
| 6 | 0.048 | 0.116 | 0.216 | 0.341 | 0.479 | 0.616 | 0.739 | 0.839 | 0.911 | 0.957 | 0.982 |
| 7 | 0.002 | 0.009 | 0.025 | 0.055 | 0.102 | 0.167 | 0.249 | 0.345 | 0.450 | 0.557 | 0.661 |
| 8 | 2.3×10^{-4} | 0.001 | 0.005 | 0.012 | 0.025 | 0.046 | 0.077 | 0.119 | 0.173 | 0.238 | |
| 9 | | 2.9×10^{-5} | 2.0×10^{-4} | 0.001 | 0.002 | 0.005 | 0.011 | 0.020 | 0.034 | 0.053 | |
| 10 | | | 3.2×10^{-6} | 2.5×10^{-5} | 1.1×10^{-4} | 3.6×10^{-4} | 0.001 | 0.002 | 0.004 | 0.008 | |
| 11 | | | | 3.2×10^{-7} | 2.8×10^{-6} | 1.4×10^{-5} | 4.9×10^{-5} | 1.4×10^{-4} | 3.5×10^{-4} | 0.001 | |
| 12 | | | | | 2.7×10^{-8} | 2.7×10^{-7} | 1.5×10^{-6} | 5.8×10^{-6} | 1.8×10^{-5} | 5.0×10^{-5} | |
| 13 | | | | | | 2.0×10^{-9} | 2.2×10^{-8} | 1.3×10^{-7} | 5.6×10^{-7} | 1.9×10^{-6} | |
| 14 | | | | | | | 1.2×10^{-10} | 1.4×10^{-9} | 9.2×10^{-9} | 4.3×10^{-8} | |
| 15 | | | | | | | | 5.2×10^{-12} | 6.9×10^{-11} | 4.9×10^{-10} | |
| 16 | | | | | | | | | 1.6×10^{-13} | 2.3×10^{-12} | |

Data Availability Statement

Daily streamflow and precipitation data are available at <https://doi.org/10.5281/zenodo.3709337>. Daily evaporation data from ERA5 are available at <https://cds.climate.copernicus.eu/datasets/reanalysis-era5-single-levels?tab=overview>. The analyses were conducted with the R packages sandwich (Zeileis et al., 2020), raster (Hijmans & van Etten, 2012), sf (Pebesma, 2018), dplyr (Wickham et al., 2015), and ggplot2 (Wickham, 2016).

Acknowledgments

This work was supported by the Brazilian National Council for Scientific and Technological Development (CNPq) and the Foundation for Research and Innovation of the State of Santa Catarina (FAPESC). The authors would like to thank David Lun for providing the script to calculate the probabilities and for the productive discussions.

References

- ANA—Brazilian National Water Agency. (2018). Relatorio de Segurança de Barragens 2017 (p. 84).
- ANA—Brazilian National Water Agency. (2019a). Levantamento Da Agricultura Irrigada Por Pivôs Centrais No Brasil (1985–2017), 2a edição (p. 49).
- ANA—Brazilian National Water Agency. (2019b). Manual De Usos Consuntivos Da Água No Brasil (p. 75).
- Benjamini, Y., & Hochberg, Y. (1995). Controlling the false discovery rate: A practical and powerful approach to multiple testing. *Journal of the Royal Statistical Society: Series B*, 57(1), 289–300. <https://doi.org/10.1111/j.2517-6161.1995.tb02031.x>
- Bernal, J. P., Cruz, F. W., Strikis, N. M., Wang, X., Deininger, M., Catunda, M. C. A., et al. (2016). High-resolution Holocene south American monsoon history recorded by a speleothem from Botuverá Cave, Brazil. *Earth and Planetary Science Letters*, 450, 186–196. <https://doi.org/10.1016/j.epsl.2016.06.008>
- Bevacqua, A. G., Chaffee, P. L. B., Chagas, V. B. P., & AghaKouchak, A. (2021). Spatial and temporal patterns of propagation from meteorological to hydrological droughts in Brazil. *Journal of Hydrology*, 603, 126902. <https://doi.org/10.1016/j.jhydrol.2021.126902>
- Blöschl, G., Bierkens, M. F. P., Chambel, A., Cudennec, C., Destouni, G., Fiori, A., et al. (2019). Twenty-three unsolved problems in hydrology (UPH)—A community perspective. *Hydrological Sciences Journal*, 64(10), 1141–1158. <https://doi.org/10.1080/02626667.2019.1620507>
- Blöschl, G., Hall, J., Viglione, A., Perdigão, R. A. P., Parajka, J., Merz, B., et al. (2019). Changing climate both increases and decreases European river floods. *Nature*, 573(7772), 108–111. <https://doi.org/10.1038/s41586-019-1495-6>
- Blöschl, G., Kiss, A., Viglione, A., Barriendos, M., Böhme, O., Brázil, R., et al. (2020). Current European flood-rich period exceptional compared with past 500 years. *Nature*, 583(7817), 560–566. <https://doi.org/10.1038/s41586-020-2478-3>
- Bola, G. B., Tshimanga, R. M., Neal, J., Trigg, M. A., Hawker, L., Lukanda, V. M., & Bates, P. (2022). Understanding flood seasonality and flood regime shift in the Congo River Basin. *Hydrological Sciences Journal*, 67(10), 1496–1515. <https://doi.org/10.1080/02626667.2022.2083966>
- Braga, B., & Kelman, J. (2016). Facing the challenge of extreme climate: The case of metropolitan São Paulo. *Water Policy*, 18(S2), 52–69. <https://doi.org/10.2166/wp.2016.113>

- Buckley, B. M., Palakit, K., Duangsathaporn, K., Sanguantham, P., & Prasomsin, P. (2007). Decadal scale droughts over northwestern Thailand over the past 448 years: Links to the tropical Pacific and Indian ocean sectors. *Climate Dynamics*, 29(1), 63–71. <https://doi.org/10.1007/s00382-007-0225-1>
- Carvalho, L. M. V., Jones, C., Silva, A. E., Liebmann, B., & Silva Dias, P. L. (2011). The South American monsoon system and the 1970s climate transition. *International Journal of Climatology*, 31(8), 1248–1256. <https://doi.org/10.1002/joc.2147>
- Cavalcanti, I. F. A. (2012). Large scale and synoptic features associated with extreme precipitation over south America: A review and case studies for the first decade of the 21st century. *Atmospheric Research*, 118, 27–40. <https://doi.org/10.1016/j.atmosres.2012.06.012>
- Chagas, V. B. P., Chaffé, P. L. B., Addor, N., Fan, F. M., Fleischmann, A. S., Paiva, R. C. D., & Siqueira, V. A. (2020a). CAMELS-BR: Hydroclimatological time series and landscape attributes for 897 catchments in Brazil. *Earth System Science Data*, 12(3), 2075–2096. <https://doi.org/10.5194/esd-12-2075-2020>
- Chagas, V. B. P., Chaffé, P. L. B., Addor, N., Fan, F. M., Fleischmann, A. S., Paiva, R. C. D., & Siqueira, V. A. (2020b). CAMELS-BR: Hydroclimatological time series and landscape attributes for 897 catchments in Brazil—Link to files. *Zenodo*. <https://doi.org/10.5281/zenodo.3964745>
- Chagas, V. B. P., Chaffé, P. L. B., & Blöschl, G. (2022a). Climate and land management accelerate the Brazilian water cycle. *Nature Communications*, 13(1), 5136. <https://doi.org/10.1038/s41467-022-32580-x>
- Chagas, V. B. P., Chaffé, P. L. B., & Blöschl, G. (2022b). Process controls on flood seasonality in Brazil. *Geophysical Research Letters*, 49(5), 1. <https://doi.org/10.1029/2021GL096754>
- Chagas, V. B. P., Chaffé, P. L. B., & Blöschl, G. (2024). Regional low flow hydrology: Model development and evaluation. *Water Resources Research*, 60(2), e2023WR035063. <https://doi.org/10.1029/2023WR035063>
- Cook, B. I., Smerdon, J. E., Cook, E. R., Williams, A. P., Anchukaitis, K. J., Mankin, J. S., et al. (2022). Megadroughts in the common Era and the Anthropocene. *Nature Reviews Earth & Environment*, 3(11), 741–757. <https://doi.org/10.1038/s43017-022-00329-1>
- Cuartas, L. A., Cunha, A. P. M. D. A., Alves, J. A., Parra, L. M. P., Deusdará-Leal, K., Costa, L. C. O., et al. (2022). Recent hydrological droughts in Brazil and their impact on hydropower generation. *Water*, 14(4), 601. <https://doi.org/10.3390/w14040601>
- Custodio, E. (2002). Aquifer overexploitation: What does it mean? *Hydrogeology Journal*, 10(2), 254–277. <https://doi.org/10.1007/s10040-002-0188-6>
- David, P. C., Chaffé, P. L. B., Chagas, V. B. P., Dal Molin, M., Oliveira, D. Y., Klein, A. H. F., & Fenicia, F. (2022). Correspondence between model structures and hydrological signatures: A large-sample case study using 508 Brazilian catchments. *Water Resources Research*, 58(3), e2021WR030619. <https://doi.org/10.1029/2021WR030619>
- de Lavenne, A., Andréassian, V., Crochemore, L., Lindström, G., & Arheimer, B. (2022). Quantifying multi-year hydrological memory with catchment forgetting curves. *Hydrology and Earth System Sciences*, 26(10), 2715–2732. <https://doi.org/10.5194/hess-26-2715-2022>
- Di Baldassarre, G., Wanders, N., AghaKouchak, A., Kuil, L., Rangecroft, S., Veldkamp, T. I. E., et al. (2018). Water shortages worsened by reservoir effects. *Nature Sustainability*, 1(11), 617–622. <https://doi.org/10.1038/s41893-018-0159-0>
- d'Orgeville, M., & Peltier, W. R. (2007). On the Pacific decadal oscillation and the Atlantic multidecadal oscillation: Might they be related? *Geophysical Research Letters*, 34(23), L23705. <https://doi.org/10.1029/2007GL031584>
- Ekolu, J., Dieppois, B., Sidibe, M., Eden, J. M., Tramblay, Y., Villarini, G., et al. (2022). Long-term variability in hydrological droughts and floods in sub-Saharan Africa: New perspectives from a 65-year daily streamflow dataset. *Journal of Hydrology*, 613, 128359. <https://doi.org/10.1016/j.jhydrol.2022.128359>
- Flantua, S. G. A., Hooghiemstra, H., Vuille, M., Behling, H., Carson, J. F., Gosling, W. D., et al. (2016). Climate variability and human impact in south America during the last 2000 years: Synthesis and perspectives from pollen records. *Climate of the Past*, 12(2), 483–523. <https://doi.org/10.5194/cp-12-483-2016>
- Fleischmann, A. S., Siqueira, V. A., Wongchug-Correia, S., Collischonn, W., & Paiva, R. C. D. D. (2020). The great 1983 floods in south American large rivers: A continental hydrological modelling approach. *Hydrological Sciences Journal*, 65(8), 1358–1373. <https://doi.org/10.1080/02626667.2020.1747622>
- García, N. O., & Mechoso, C. R. (2005). Variability in the discharge of South American rivers and in climate. *Hydrological Sciences Journal*, 50(3), 5. <https://doi.org/10.1623/hysj.50.3.459.65030>
- Getirana, A., Libonati, R., & Cataldi, M. (2021). Brazil is in water crisis—It needs a drought plan. *Nature*, 600(7888), 218–220. <https://doi.org/10.1038/d41586-021-03625-w>
- Grimm, A. M. (2019). South American monsoon and its extremes. In *Tropical extremes* (pp. 51–93). Elsevier.
- Gudmundsson, L., Boulange, J., Do, H. X., Gosling, S. N., Grillakis, M. G., Koutoulis, A. G., et al. (2021). Globally observed trends in mean and extreme river flow attributed to climate change. *Science*, 371(6534), 1159–1162. <https://doi.org/10.1126/science.aba3996>
- Hannaford, J., Buys, G., Stahl, K., & Tallaksen, L. M. (2013). The influence of decadal-scale variability on trends in long European streamflow records. *Hydrology and Earth System Sciences*, 17(7), 2717–2733. <https://doi.org/10.5194/hess-17-2717-2013>
- Hersbach, H., Bell, B., Berrisford, P., Hirahara, S., Horányi, A., Muñoz-Sabater, J., et al. (2020). The ERA5 global reanalysis. *Quarterly Journal of the Royal Meteorological Society*, 146(730), 1999–2049. <https://doi.org/10.1002/qj.3803>
- Hijmans, R. J., & van Etten, J. (2012). raster: Geographic analysis and modeling with raster data. In *The R project for statistical computing*.
- Huang, B., Thorne, P. W., Banzon, V. F., Boyer, T., Chepurin, G., Lawrimore, J. H., et al. (2017). NOAA extended reconstructed sea surface temperature (ERSST), version 5. *NOAA National Centers for Environmental Information*, 30(8179–8205), 25.
- Ionita, M., Lohmann, G., Rimbu, N., Chelcea, S., & Dima, M. (2012). Interannual to decadal summer drought variability over Europe and its relationship to global sea surface temperature. *Climate Dynamics*, 38(1), 363–377. <https://doi.org/10.1007/s00382-011-1028-y>
- Jacques-Coper, M., & Garreaud, R. D. (2015). Characterization of the 1970s climate shift in South America. *International Journal of Climatology*, 35(8), 2164–2179. <https://doi.org/10.1002/joc.4120>
- Kayano, M. T., Andreoli, R. V., & Ferreira de Souza, R. A. (2013). Relations between ENSO and the South Atlantic SST modes and their effects on the South American rainfall. *International Journal of Climatology*, 33(8), 2008–2023. <https://doi.org/10.1002/joc.3569>
- Kiem, A. S., & Franks, S. W. (2004). Multi-decadal variability of drought risk, eastern Australia. *Hydrological Processes*, 18(11), 2039–2050. <https://doi.org/10.1002/hyp.1460>
- Kundzewicz, Z. W., Szwed, M., & Pińskwar, I. (2019). Climate variability and floods—A global review. *Water*, 11(7), 1399. <https://doi.org/10.3390/w11071399>
- Lima, C. H. R., & AghaKouchak, A. (2017). Droughts in Amazonia: Spatiotemporal variability, teleconnections, and seasonal predictions. *Water Resources Research*, 53(12), 10824–10840. <https://doi.org/10.1002/2016WR020086>
- Liu, J., & Zhang, Y. (2017). Multi-temporal clustering of continental floods and associated atmospheric circulations. *Journal of Hydrology*, 555, 744–759. <https://doi.org/10.1016/j.jhydrol.2017.10.072>

- Lun, D., Fischer, S., Viglione, A., & Blöschl, G. (2020). Detecting flood-rich and flood-poor periods in annual peak discharges across Europe. *Water Resources Research*, 56(7), e2019WR026575. <https://doi.org/10.1029/2019WR026575>
- MacKinnon, J. G., & White, H. (1985). Some heteroskedasticity-consistent covariance matrix estimators with improved finite sample properties. *Journal of Econometrics*, 29(3), 305–325. [https://doi.org/10.1016/0304-4076\(85\)90158-7](https://doi.org/10.1016/0304-4076(85)90158-7)
- Makkonen, L., & Pajari, M. (2014). Defining sample quantiles by the true rank probability. *Journal of Probability and Statistics*, 2014, 326579. <https://doi.org/10.1155/2014/326579>
- Marengo, J. A., Souza, C. M. J., Thonicke, K., Burton, C., Halladay, K., Betts, R. A., et al. (2018). Changes in climate and land use over the Amazon region: Current and future variability and trends. *Frontiers in Earth Science*, 6, 228. <https://doi.org/10.3389/feart.2018.00228>
- Marengo, J. A., Torres, R. R., & Alves, L. M. (2017). Drought in Northeast Brazil—Past, present, and future. *Theoretical and Applied Climatology*, 129(3–4), 1189–1200. <https://doi.org/10.1007/s00704-016-1840-8>
- Markonis, Y., & Koutsoyiannis, D. (2016). Scale-dependence of persistence in precipitation records. *Nature Climate Change*, 6(4), 399–401. <https://doi.org/10.1038/nclimate2894>
- McCabe, G. J., Betancourt, J. L., Gray, S. T., Palecki, M. A., & Hidalgo, H. G. (2008). Associations of multi-decadal sea-surface temperature variability with US drought. *Quaternary International*, 188(1), 31–40. <https://doi.org/10.1016/j.quaint.2007.07.001>
- McFadden, D. (1973). Conditional logit analysis of qualitative choice behavior.
- McMillan, H. (2022). A taxonomy of hydrological processes and watershed function. *Hydrological Processes*, 36(3), e14537. <https://doi.org/10.1002/hyp.14537>
- Merz, B., Nguyen, V. D., & Vorogushyn, S. (2016). Temporal clustering of floods in Germany: Do flood-rich and flood-poor periods exist? *Journal of Hydrology*, 541, 824–838. <https://doi.org/10.1016/j.jhydrol.2016.07.041>
- Milly, P. C. D., Betancourt, J., Falkenmark, M., Hirsch, R. M., Kundzewicz, Z. W., Lettenmaier, D. P., et al. (2015). On Critiques of “Stationarity is Dead: Whither water management?” *Water Resources Research*, 51(9), 7785–7789. <https://doi.org/10.1002/2015WR017408>
- Morales, M. S., Cook, E. R., Barchivich, J., Christie, D. A., Villalba, R., LeQuesne, C., et al. (2020). Six hundred years of South American tree rings reveal an increase in severe hydroclimatic events since mid-20th century. *Proceedings of the National Academy of Sciences*, 117(29), 16816–16823. <https://doi.org/10.1073/pnas.2002411117>
- Mtilatila, L., Bronstert, A., Bürger, G., & Vormoor, K. (2020). Meteorological and hydrological drought assessment in Lake Malawi and Shire River basins (1970–2013). *Hydrological Sciences Journal*, 65(16), 2750–2764. <https://doi.org/10.1080/02626667.2020.1837384>
- Newman, M., Alexander, M. A., Ault, T. R., Cobb, K. M., Deser, C., Di Lorenzo, E., et al. (2016). The Pacific decadal oscillation, revisited. *Journal of Climate*, 29(12), 4399–4427. <https://doi.org/10.1175/JCLI-D-15-0508.1>
- O’Connell, E., O’Donnell, G., & Koutsoyiannis, D. (2022). On the spatial scale dependence of long-term persistence in global annual precipitation data and the Hurst Phenomenon. *Water Resources Research*, 59(4), e2022WR033133. <https://doi.org/10.1029/2022wr033133>
- Pebesma, E. J. (2018). Simple features for R: Standardized support for spatial vector data. *The R Journal*, 10(1), 439. <https://doi.org/10.32614/RJ-2018-009>
- Ponce, V. M. (1995). Management of droughts and floods in the semiarid Brazilian northeast—The case for conservation. *Journal of Soil and Water Conservation*, 50(5), 422–431.
- Renard, B., Lang, M., Bois, P., Dupeyrat, A., Mestre, O., Niel, H., et al. (2008). Regional methods for trend detection: Assessing field significance and regional consistency. *Water Resources Research*, 44(8), 2007WR006268. <https://doi.org/10.1029/2007WR006268>
- Renard, B., & Thyre, M. (2019). Revealing hidden climate indices from the occurrence of hydrologic extremes. *Water Resources Research*, 55(9), 7662–7681. <https://doi.org/10.1029/2019WR024951>
- Renard, B., Thyre, M., McInerney, D., Kavetski, D., Leonard, M., & Westra, S. (2022). A hidden climate indices modeling framework for Multivariable space-time data. *Water Resources Research*, 58(1), e2021WR030007. <https://doi.org/10.1029/2021WR030007>
- Saurral, R. I., Camillon, I. A., & Barros, V. R. (2017). Low-frequency variability and trends in centennial precipitation stations in southern South America. *International Journal of Climatology*, 37(4), 1774–1793. <https://doi.org/10.1002/joc.4810>
- Seager, R. (2015). Decadal hydroclimate variability across the Americas. In C.-P. Chang, M. Ghil, M. Latif, & J. M. Wallace (Eds.), *World Scientific Series on Asia-Pacific weather and climate* (Vol. 6, pp. 235–254). World Scientific. https://doi.org/10.1142/9789814579933_0015
- Slater, L., Villarini, G., Archfield, S., Faulkner, D., Lamb, R., Khouakhi, A., & Yin, J. (2021). Global changes in 20-year, 50-year, and 100-year river floods. *Geophysical Research Letters*, 48(6), e2020GL091824. <https://doi.org/10.1029/2020GL091824>
- Tarasova, L., Lun, D., Merz, R., Blöschl, G., Basso, S., Bertola, M., et al. (2023). Shifts in flood generation processes exacerbate regional flood anomalies in Europe. *Communications Earth & Environment*, 4(1), 1–12. <https://doi.org/10.1038/s43247-023-00714-8>
- Tedeschi, R. G., Grimm, A. M., & Cavalcanti, I. F. A. (2015). Influence of Central and East ENSO on extreme events of precipitation in South America during austral spring and summer. *International Journal of Climatology*, 35(8), 2045–2064. <https://doi.org/10.1002/joc.4106>
- Tomasella, J., Cunha, A. P. M. A., Simões, P. A., & Zeri, M. (2022). Assessment of trends, variability and impacts of droughts across Brazil over the period 1980–2019. *Natural Hazards*. <https://doi.org/10.1007/s11069-022-05759-0>
- Van Loon, A. F. (2015). Hydrological drought explained. *WIREs Water*, 2(4), 359–392. <https://doi.org/10.1002/wat2.1085>
- Van Loon, A. F., & Van Lanen, H. A. J. (2012). A process-based typology of hydrological drought. *Hydrology and Earth System Sciences*, 16(7), 1915–1946. <https://doi.org/10.5194/hess-16-1915-2012>
- Vuille, M., Burns, S. J., Taylor, B. L., Cruz, F. W., Bird, B. W., Abbott, M. B., et al. (2012). A review of the South American monsoon history as recorded in stable isotopic proxies over the past two millennia. *Climate of the Past*, 8(4), 1309–1321. <https://doi.org/10.5194/cp-8-1309-2012>
- Wickham, H. (2016). *ggplot2: Elegant graphics for data analysis*. Springer-Verlag.
- Wickham, H., François, R., Henry, L., & Müller, K. (2015). dplyr: A grammar of data manipulation. In *The R Project for Statistical Computing*.
- Wilks, D. S. (2006). On “field significance” and the false discovery rate. *Journal of Applied Meteorology and Climatology*, 45(9), 1181–1189. <https://doi.org/10.1175/JAM2404.1>
- Wilks, D. S. (2016). “The stippling shows statistically significant grid Points”: How research results are routinely overstated and overinterpreted, and what to do about it. *Bulletin of the American Meteorological Society*, 97(12), 2263–2273. <https://doi.org/10.1175/BAMS-D-15-00267.1>
- Zeileis, A., Kölle, S., & Graham, N. (2020). Various versatile variances: An object-oriented implementation of clustered covariances in R. *Journal of Statistical Software*, 95, 1–36. <https://doi.org/10.18637/jss.v095.i01>